

Surface functionalisation by the introduction of self-healing properties

into electroless Ni-P coatings

Alicja Stankiewicz^{*1}, Zoi Kefallinou², Grzegorz Mordarski³, Zofia Jagoda⁴, Ben Spencer²

¹Edinburgh Napier University, School of Engineering and the Built Environment, 10 Colinton Road, Edinburgh, EH10 5DT, UK

²University of Manchester, School of Materials, Oxford Road, Manchester, M13 9PL, UK

³Jerzy Haber Institute of Catalysis and Surface Chemistry, Polish Academy of Sciences, Niezapominajek 8, PL-30239 Krakow, Poland

⁴Wroclaw University of Economics, Faculty of Engineering and Economics, Komandorska 118-120, PL-53345 Wroclaw, Poland

*corresponding author: a.stankiewicz@napier.ac.uk

Abstract

Ni-P\alginate microgels coatings, as potential metallic protective coatings with self-healing properties, were deposited by the electroless method. The alginate microgels contained nickel chloride and sodium hypophosphite. It was proven that the reduction of nickel ions released from the microgels is possible on the steel and Ni-P coating surface. The self-healing effect of this system was studied by X-ray fluorescence (XRF), chronoamperometry and scanning vibrating electrode technique (SVET). An improved corrosion protection observed here is attributed to the reduction of nickel ions to metallic nickel on the tested surfaces. Differences in the surface concentration of nickel and phosphorous species in the corrosion tested coatings with and without microgels, as evaluated using X-ray Photoelectron Spectroscopy (XPS), provided substantial evidence for the formation of a Ni-P coating from the compounds included in the microgels.

Keywords: self-healing coating, Ni-P coating, corrosion resistance, alginate microgels, SVET, XPS, XRF

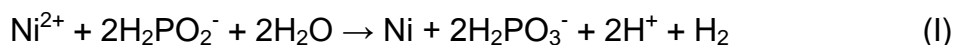
1. Introduction

The provision of robust, durable, low-cost, protective coatings is of benefit to local and global economic growth across many industrial sectors. A beneficial feature of a relatively new category of advanced coating material is the ability to self-heal. Self-healing protective coatings investigated so far are mainly based on carrier systems that store self-healing substances [1–7], and most often capsules or fibres are included in the polymeric matrices [6,8–12]. Many polymer-based materials have been used in this role, however, compared with materials based on metals or ceramics, polymeric coatings have poor mechanical properties, which limits their applications.

The carcinogenic hexavalent chromium, was, until recently, a key compound employed in research into self-healing metallic coatings. In the context of wear resistance, hardness and corrosion resistance, nickel-phosphorous (Ni-P) coatings are comparable to chromium coatings. Although Ni-P coatings do not currently have the ability to regenerate, a viable solution to this problem is the encapsulation of corrosion inhibitors and the introduction of the capsules into the matrix of the coating. This approach has been described for electrochemically-generated nickel [13] and zinc [14] coatings. In the case of the nickel coating prepared nanocontainers did not contain any active substances. The self-healing protective zinc coating contained nanoaggregates of polyethylene oxide-b-polystyrene (PEO₁₁₃-b-PS₂₁₈). The self-healing properties of these systems resulted from the ability of amphiphilic polymers to shrink and swell reversibly.

A new nickel-phosphorous self-healing coating process, which promises enhanced material properties and a low toxicity production process compared to the chromium-based equivalent is proposed [15]. The introduction of microgels comprised of nickel salts and sodium hypophosphite into Ni-P matrices results in the surface functionalisation by the introduction of

self-healing properties. The reconstruction of a metallic coating at the time of damage is possible due to the autocatalytic reaction of nickel and phosphorous deposition [16]:



XRF, chronoamperometry and SVET were used to study the self-healing effect. The morphology of the Ni-P and Ni-P\alginate microgels coatings was examined by scanning electron microscope (SEM) and fluorescence microscope. The elemental and chemical composition of the coatings was performed by energy dispersive X-ray spectroscopy (EDX) and XPS.

2. Materials and methods

2.1 Materials

For microgels preparation, alginic acid sodium salt from brown algae, paraffin oil, Span 80, sodium hypophosphite, nickel chloride, fluorescein and acetone were used. For the electroless deposition of nickel-based coatings nickel chloride, sodium hypophosphite, sodium citrate and sodium hydroxide were used. Watt's bath containing nickel sulphate, nickel chloride and boric acid was used to produce thin nickel coatings for a proof of concept trial. NaCl solution was used for corrosion resistance analysis, Scanning Vibrating Electrode Technique (SVET) tests and X-ray Photoelectron Spectroscopy (XPS) analysis. All materials were purchased from Sigma Aldrich and were used without further purification.

1
2
3
4
5
6
7
8
9
10
11
12
13
14
15
16
17
18
19
20
21
22
23
24
25
26
27
28
29
30
31
32
33
34
35
36
37
38
39
40
41
42
43
44
45
46
47
48
49
50
51
52
53
54
55
56
57
58
59
60
61
62
63
64
65

The specimens of A1008 steel of different sizes dictated by the requirements of the testing method were used. The steel surface was ground from 600 to 1200 grit silicon carbide abrasive paper, then washed with detergent and then rinsed with deionised water and acetone.

2.2 Alginate microgels production

For proof of concept trials, the intention was to produce large alginate microgels to provide a high amount of sodium hypophosphite and nickel chloride. 3 wt.% solution of sodium salt of alginic acid was stirred with 3 mol dm⁻³ solution of sodium hypophosphite. This mixture was added dropwise to 2 mol dm⁻³ solution of nickel chloride. In this way, microgels with diameters up to 5 mm were produced.

Alginate microgels for co-deposition with nickel-based coating were produced by a reverse emulsion method. 3 wt.% solution of sodium salt of alginic acid was mixed with 3 mol dm⁻³ solution of sodium hypophosphite and 1 x 10⁻³ mol dm⁻³ solution of fluorescein (i.e., to allow detection of microgels in coatings under a fluorescent microscope). This mixture was added dropwise to oil phase (paraffin oil with Span 80). After 15 minutes of stirring 2 mol dm⁻³ solution of nickel chloride was added dropwise. Separation of oil phase was performed by vacuum filtration with use of acetone as a drying agent. Microgels with a diameter of up to 5 µm were obtained.

2.3 Deposition of nickel coatings

Electroplating of nickel coatings on steel samples was carried out for proof of concept trials. A part of a steel substrate was covered by varnish 'Slotowax' to provide a working surface of 3 cm². The deposition of nickel was performed from the Watt's bath at room temperature. The

bath contained, at g dm^{-3} : nickel chloride 150, nickel sulphate 180, and boric acid 50. The current density was of 0.05 A cm^{-2} . Deposition time was of 20 s.

Electroless deposition of Ni-P coatings was carried out on steel samples $35 \times 25 \times 0.5 \text{ mm}$ from a bath containing, at g dm^{-3} : nickel chloride 36, sodium hypophosphite 26, sodium citrate 44. The pH was adjusted to 9 by 10 wt.% solution of NaOH. The temperature of deposition was 60°C for the first 10 minutes of deposition and then 40°C thereafter, and the total time of deposition was of 2 hours. To produce Ni-P\alginate microgels coatings, alginate microgels were added to the bath after 10 minutes of Ni-P coating deposition at 60°C . During the deposition process, the pH was checked at 15 minute intervals and adjusted to the initial value if necessary. Coatings of thickness $10.0 \pm 0.7 \mu\text{m}$ were produced.

2.4 Proof of concept test

Steel specimens covered with thin, uneven layer of electroplated nickel coating (*i.e.*, the only area of 3 cm^2 was exposed) were immersed in 50 ml of 3.5 wt.% NaCl solution with and without large microgels. The amount of microgels added to the NaCl solution was 18 grams. Immersion tests were carried out in 3.5 wt.% solution of NaCl at room temperature for 72 hours.

2.5 Microscopic analysis of Ni-P and Ni-P\alginate microgels coatings

The surface morphology and composition of the deposited coatings were examined using a Scanning Electron Microscope (SEM) equipped with energy dispersive X-ray spectroscopy (EDX) - VEGA II SBH.

The presence of alginate microgels in the Ni-P matrix was detected by a fluorescent microscope -Olympus BX53M.

2.6 X-ray fluorescence analysis

1 X-ray fluorescence (XRF) was used to analyse the nickel content on the steel substrates. The
2
3 XRF measurements were carried out on an EDX 3600 H Skyray instrument. Elemental
4
5 analysis of the steel specimen composition was performed before and after 1, 3 and 24 hours
6
7 of immersion in 3.5 wt.% solution of NaCl.
8
9

2.7 Electrochemical analysis

10
11
12
13
14
15
16
17
18 Chronoamperometry measurements were done using a combined
19
20 Potentiostat/Galvanostat/EIS Analyzer PARSTAT 4000 AMETEK. The measurements were
21
22 carried out in 100 cm³ of 3.5 wt.% NaCl solution using a three-electrode electrochemical cell.
23
24 The steel element with an exposure area of 3 cm² served as the working electrode. The
25
26 counter electrode was a platinum foil, and the reference electrode was silver/silver chloride
27
28 electrode. To force the corrosion process a potential polarisation of 10mV above the open
29
30 circuit potential was applied. After 600 s of the measurement 18 grams of the large alginate
31
32 microgels were added to the solution. The test was performed for 1 hour.
33
34
35
36
37
38
39

40 For the scanning vibrating electrode technique measurements, samples were mounted in
41
42 epoxy-resin, leaving the coating surface exposed to be examined, and having an electrical
43
44 connection attached on its backside, for the connection to the electrochemical equipment. The
45
46 sample edges were sealed using a beeswax/colophony mixture (3:1), and the sample was
47
48 mounted in a glass cell that allowed it to remain at a stable, levelled position. The SVET
49
50 measurements were performed on a Uniscan M370 Electrochemical Workstation with an
51
52 automated stage control. The probe employed consisted of a 5-100 µm Pt-Ir wire that was
53
54 positioned at 100 µm above the sample surface. The distance between the probe tip and the
55
56 sample surface was calculated using the reflection of the tip on the metallic sample with the
57
58
59
60
61
62
63
64
65

1
2
3
4
5
6
7
8
9
10
11
12
13
14
15
16
17
18
19
20
21
22
23
24
25
26
27
28
29
30
31
32
33
34
35
36
37
38
39
40
41
42
43
44
45
46
47
48
49
50
51
52
53
54
55
56
57
58
59
60
61
62
63
64
65

help of a microscope. The probe was then set to vibrate with a 30 μm amplitude perpendicular to the sample surface at 80 Hz and to scan the sample surface at 100 μm steps. The electrolyte selected for these tests was $50 \times 10^{-3} \text{ mol dm}^{-3}$ aqueous NaCl solution at room temperature, as the current sensitivity of the specific system, has been found to improve in a solution of low conductivity. After adding the electrolyte, the glass cell was sealed using a gasket to reduce any conductivity changes caused by electrolyte evaporation during the duration of the test. Finally, since SVET is highly sensitive to the probe sensitivity, the vibration amplitude, the solution conductivity and the selected distance between the probe and the sample, it is essential that a calibration factor is estimated for each test, which allows conversion of the recorded potential into current density values. This was achieved by mapping the potential response of a 200 μm diameter epoxy-mounted gold wire under galvanostatic control, using the same probe and testing conditions as for the Ni-P samples. The SVET measurements were taken after 0, 5, 12, 18 and 20 h of the immersion.

2.8 X-ray Photoelectron Spectroscopy analysis

X-ray Photoelectron Spectroscopy was performed using an Axis Ultra Hybrid spectrometer (Kratos Analytical, Manchester, UK) using a monochromated Al K_{α} X-ray source (1486.6 eV, 150 W). Survey spectra were measured using an analyser pass energy of 80 eV, and 20 eV pass energy was used for high-resolution spectra. A fast snapshot spectrum of the Ni 2p_{3/2} core level was used to optimise the sample position. A charge neutraliser was used to remove any differential charging caused by a poor conductive connection to the sample plate. Measurements were carried out under ultra-high vacuum with a base pressure $\sim 1 \times 10^{-8}$ mbar. Survey spectra showed small amounts of several other elements (varying with sample) including Na, Zn, N, and Si.

The XPS spectra were fit with product-approximation Voigt functions (convoluted Gaussian-Lorentzian peaks) using CasaXPS (www.casaxps.com). Charge calibration was performed using the hydrocarbon component of the C 1s photoelectron peak at 284.8 eV. Shirley backgrounds were applied to the spectra, with an offset at the high binding energy position in the case of Ni 2p as prescribed by Biesinger *et al.* [17].

3. Results and discussion

3.1 Proof of concept trials

Steel specimens covered with thin, uneven layer of electroplated nickel coating (*i.e.*, only an area of 3 cm² was exposed) were immersed in 50 ml of 3.5 wt.% NaCl solution with and without large microgels for 72 hours. The reason for the coverage of the steel samples with nickel coating was to simulate the impaired nickel coating. Figure 1 shows a photograph of samples after 24 hours of immersion. The sample immersed in NaCl solution without microgels (bottom sample) suffered severe corrosion. Brownish corrosion products of iron were visible. The sample immersed in the solution with microgels (top) did not exhibit corrosion for the whole duration of the experiment.

To check if the deposition of nickel is possible under these conditions, the steel sample without any coating was immersed in the solution of 3.5 wt.% NaCl containing large alginate microgels for 24 hours. XRF was used to analyse the nickel content on the steel substrates. The measurements were taken before and after 1, 3 and 24 hours of immersion. The results are presented in Table 1. The nickel content on the steel surface grew from 0 and increased to 2.3% after 24h. The fastest growth was observed after the first hour of immersion in NaCl solution. These results show that the release of nickel chloride and sodium hypophosphite, as

well as the deposition of nickel on the steel substrate, in a NaCl solution at room temperature is possible.

1
2
3
4 Additionally, chronoamperometry was used to accelerate the corrosion process and evaluate
5
6 the inhibiting effect of the alginate microgels on the steel substrate in a NaCl solution. The
7
8 chronoamperometric results showed a decrease in the current flow of the steel surface
9
10 exposed to the NaCl solution containing microgels compared to the solution without microgels,
11
12 as shown in Figure 2. The sudden increase in the current flow at 600 s is caused by the
13
14 addition of alginate microgels to the solution. The corrosion inhibition efficiency (η) was
15
16 calculated from the following equation [18]:
17
18
19
20
21
22

$$\eta = 100 \times \left(1 - \frac{j}{j_0}\right) \quad (1)$$

23
24
25
26
27
28
29 where j and j_0 are the corrosion current densities at the time of 3600 s in the presence and
30
31 absence of the microgels, respectively. The corrosion inhibition efficiency was calculated at
32
33 48%.
34
35

36
37 The successful outcomes of this proof of concept research led to the design of nickel-based
38
39 coatings with self-healing properties, and the preparation of Ni-P coatings with alginate
40
41 microgels filled with nickel chloride and sodium hypophosphite was the next step.
42
43
44
45

46 *3.2 Microscopic analysis of Ni-P and Ni-P\alginate microgels coatings*

47
48
49
50

51 Figure 3 shows SEM micrographs of the surface of the Ni-P and Ni-P\alginate microgels
52
53 coatings. The surface morphology was typical for Ni-P deposits and exhibited a cauliflower-like
54
55 appearance [19]. The Ni-P\alginate microgels coatings had a smoother surface compared with
56
57 the plain Ni-P coating. Furthermore, there were some holes on the surface of the composite
58
59 coatings. An EDX point analysis revealed a relatively high carbon concentration at these holes.
60
61
62
63
64
65

This could mean that the holes were remainings after alginate microgels, which could be destroyed due to low pressure in the microscope. The composition of the Ni-P and Ni-P\alginate microgels coatings were 4.7 and 5.1 wt.% of P, respectively. The composition of the holes was of 79.1 wt.% Ni, 16.7 wt.% C and 4.2 wt.% P. In spite of the large size, the microgels did not generate voids or defects in the Ni-P matrix.

Figure 4 presents fluorescent microgels on the surface of the Ni-P\alginate microgels coating. The spherical microgels with diameters up to 5 μm were observed. The microgels were filled with fluorescein, so a green fluorescence was expected. However, yellow and red fluorescence was also visible, and could be caused by the nature of the sodium alginate obtained from brown algae. Sodium alginate is strongly fluorescent due to small amounts of polyphenolic residues. The emission signal for these compounds was observed in the range of 400-900 nm [20,21].

3.3 SVET analysis of the coatings

Figure 5 shows the current density changes that took place in the electrolyte above the coating surfaces after 0, 5, 12, 18 and 20 h immersion in 50mM NaCl. In this setup, the positive current values represented anodic current direction, while the negative represented cathodic direction. Initially (0h), the whole sample surface appeared neutral, and no activity was recorded above it, as the Ni-P coating layer was acting as a continuous protective barrier, Fig. 5a. After 5h immersion, though, a broad anodic response was recorded developing on the right side of the map, suggesting corrosion initiation. A few hours later (12h), the first signs of cathodic activity appeared on the left side of the map at a remote distance from the anodic region.

Simultaneously, the anodic area shrank into a more localised region, but its intensity was not reduced. Since the current density around the anodic region was high, it is possible that the coating was destroyed and steel corrosion was taking place instead. Since the Ni-P coating is

cathodic with respect to steel, its cathodic character is better observed only after corrosion of steel the substrate has already initiated.

1
2 On the other hand, the current densities recorded on the Ni-P\alginate microgels sample (Fig.
3
4 5b) on the beginning of immersion were one order of magnitude lower than the current density
5
6 found on the Ni-P coating, suggesting that the alginate microgels reduced the corrosion rate of
7
8 the coating. The first detected reaction at the beginning of immersion, in this case, was a
9
10 broadly spread cathodic response. This cathodic current may have been originating from the
11
12 nickel reduction occurring during nickel chloride and sodium hypophosphate release from the
13
14 microgels and appeared to take place immediately after immersion in the electrolyte. The
15
16 nickel content growth on the steel substrate immersed in NaCl solution was also detected by
17
18 XRF method. This behaviour could indicate a self-healing activity of the coating containing the
19
20 alginate microgels due to the autocatalytic reaction of nickel and phosphorous deposition. The
21
22 imbalance of cathodic and anodic currents at the beginning of the immersion in the NaCl
23
24 solution was observed. It can be explained as follows:
25
26
27
28
29
30

- 31 i. SVET only measures net ionic fluxes, and if one activity dominates over other, the
32
33 resulting net current shown by SVET is anodic or cathodic [22].
34
35
- 36 ii. The current density can become smaller than the limit of detection when one activity is
37
38 so localised that it is easily detected, while the other one is spread through the rest of
39
40 the surface [23].
41
42
- 43 iii. The cathodic reaction results in the nickel-phosphorous coating by reduction of nickel
44
45 and phosphorous, which is a process adhering to a place where the microgels are
46
47 present. The anodic reaction, oxidation of the reducer, creates ionic products, which can
48
49 flow smoothly.
50
51
52
53

54
55 The cathodic activity was not maintained. With longer immersion, as the microgels content in
56
57 that area was leaching, the initial strong cathodic response became less intense (5h). After 12h
58
59 immersion, the sample was mostly neutral, and at the earlier cathodic region, evidence of small
60
61
62
63
64
65

interchanging anodic/cathodic activity was seen. This behaviour remains stable until 20 h later. At this point, the autocatalytic deposition of the Ni-P coating was finished, because of exhausting of all substrates from the microgels. However, the microgels themselves can be an effective inhibitor of steel substrates corrosion [24,25]. The alginate derivatives follow a mixed inhibition mechanism. The alginate may be adsorbed on the cathodic sites of carbon steel, and this inhibits the cathodic hydrogen evolution reaction. On the other hand, –OH groups have lone pairs of electrons and can be adsorbed on the anodic sites, what inhibits the anodic metal dissolution reaction [25]. The corrosion current above active sites was considerably low and did not appear to lead to any further corrosion within the exposure time. This suggests that the initial cathodic current was only caused by reactions on the surface of the nickel coating surface, which were not as destructive as the galvanic current between steel and nickel in case of the Ni-P sample.

3.4 XPS analysis of the coatings

Ni 2p photoelectron spectra, like other transition metals, are complex and influenced by a variety of multiplet, shake-up and plasmon loss structures [17,26]. The approach as outlined by Biesinger *et al.* was followed to fit multiple peaks for NiP (principle peak at 852.6 eV binding energy), NiO (principle peak at 853.7 eV) and Ni(OH)₂ (principle peak at 855.3 eV), where for a lot of the spectra, all three species (with several associated peaks with well-defined binding energy shifts and area intensity ratios [17]) were required to obtain an adequate and consistent fit across the whole dataset. A more holistic approach is often taken to first row transition metal 2p spectra, given that the complexity of the spectra can create a relatively large amount of uncertainty. In this approach, a minimal number of principle peaks are applied to the spectral envelope to identify the amount of metallic nickel (or in this case NiP), oxide or hydroxide species [27–29], typically over the binding energy region of 850-860 eV. However, given the complex satellite structure to higher binding energy exhibited by oxide species, a more

thorough peak fitting is required to achieve an accurate determination of the prevalence of each chemical species [17,26], which was the approach taken here, and it should be noted that all binding energy positions found for each chemical species were all in good agreement with other literature values for NiP, oxide and hydroxide [27].

Figure 6 shows the Ni $2p_{3/2}$ spectrum for Ni-P coating in the as-deposited state, where multiple peaks associated with NiP, NiO and Ni(OH)₂ as outlined by Biesinger *et al.* were required to obtain an adequate fit [17]. This fit was consistently applied to all the spectra of Ni-P and Ni-P\alginate microgels coatings with the percentage of each chemical species varying. Consistently NiP and Ni(OH)₂ were required to obtain a good fit in all samples, although some samples exhibited no NiO.

Figure 7 shows the comparison of the spectra for Ni-P and Ni-P\alginate microgels coatings at their as-deposited state. Two peaks in the Ni $2p_{3/2}$ spectrum, one at 852.3 eV (mainly associated with NiP) and ~856 eV (mainly associated with hydroxide) changed slightly. Both coatings consisted mainly of NiP. There was less Ni in general in the coating with microgels compared to the plain nickel coating. Nickel content (Table 2) was 3.11 % for the latter one and 0.79%, with more carbon signal seen, for Ni-P\alginate microgels. Thus, it can indicate the existence of alginate microgels filled with nickel salt in the Ni-P matrix.

The P $2p$ spectra for Ni-P coating in the as-deposited state were consistently fit with two doublets (with a spin-orbit splitting of 0.88 eV) as shown in Figure 8 with binding energy positions ($2p_{3/2}$) at 129.4 eV and 132.4 eV associated with phosphide and phosphate (i.e., oxidised) species respectively, again in agreement with literature values [27–29]. The O $1s$ spectra were found to contain a chemical species associated with Ni(OH)₂ at a binding energy of ~531 eV associated with hydroxide [29,30], although the oxygen spectra were convoluted by chemical species associated with carbon oxide contamination at similar binding energies. The

amount of phosphorous oxidation was calculated from the ratio of the fitted phosphide and phosphate species in the P 2p spectra; consistently there was less phosphate compared to phosphide (i.e., there was less oxidation) than that exhibited by Ni. Notably, all the samples showed some amount of phosphate.

The Ni:P ratio (calculated using the peak areas of the Ni 2p and P 2p spectra, after normalising to the relative sensitivity factor- mainly influenced by the difference in photoionisation cross section), for different times of immersion in NaCl solution, is presented in Table 2. In the case of Ni-P coatings, the ratio was increasing with immersion time and correlated with the amount of nickel oxidation in the Ni-P coating. The increase of the concentration of the oxidised nickel species is due anodic dissolution of the coating. According to J. Kang *et al.*, in an alkaline solution anodic oxidation of Ni is accompanied by another anodic reaction. In this case, phosphorous is also oxidised. Both P and PO_x can react with a corrosive solution and can be removed from the coating surface [31]. The contribution of alloying P to the dissolution process of Ni-P coatings in NaCl solution was also observed by Krolkowski *et al.* [32]. For Ni-P\alginate microgels, the Ni:P ratio did not change significantly with time of immersion in NaCl solution. There was almost no change in amount in NiP in the Ni-P\alginate microgels coating. Figure 9 shows the comparison between the Ni 2p_{3/2} spectra for Ni-P and Ni-P\alginate microgels coatings after 6 h of immersion in NaCl solution.

The increase of the amount of P and the maintenance of the amount of NiP (i.e., in chemical analysis) with the immersion time of Ni-P\alginate microgels coatings in NaCl solution is evidence of the process of electroless deposition of nickel on tested samples.

4. Conclusions

The alginate microgels were successfully synthesised. They are promising candidates as carriers of nickel chloride and sodium hypophosphite for the Ni-P coating functionalisation. The results of XRF analysis proved that reduction of nickel ions released from the microgels on the

steel surface is possible. Chronoamperometry measurements showed the beneficial effect of the alginate microgels on the corrosion performance of the steel substrate.

1
2 It was demonstrated that the microgels could be co-deposited with the nickel matrix by the
3
4 electroless plating method. The microgels with the diameter of up to 5 μm were detected by
5
6 scanning electron microscopy and fluorescence microscopy. The co-deposited microgels did
7
8 not influence the chemical composition of the nickel matrix.
9
10

11
12 The Ni-P\alginate microgels coatings exhibited enhanced corrosion protection in comparison to
13
14 the Ni-P coatings, as determined with SVET testing, by reducing the current density
15
16 produced at the sample surface upon immersion. Additionally, the Ni-P\alginate microgels
17
18 coating did not demonstrate any intense, highly localised anodic sites development as the Ni-P
19
20 sample, indicating that the presence of the microgels delays any significant degradation of the
21
22 Ni-P layer that led to the exposure of steel to the corrosive environment. The SVET analysis
23
24 confirmed that the Ni-P\alginate microgels coating therefore has self-healing properties.
25
26
27

28
29 The difference in chemical composition of the passive layer on the surfaces of the coatings
30
31 with and without microgels was identified by XPS. Oxidised nickel and phosphorous
32
33 compounds were present in all samples. The amount of the oxidised species increased with
34
35 the time of immersion in NaCl solution in the Ni-P coatings. There was almost no change in the
36
37 amount of oxidised nickel compounds, and there was a decrease in the amount of
38
39 phosphorous oxides in the Ni-P\alginate microgels coatings.
40
41
42

43
44 It is important to highlight that the reconstruction effect based on the autocatalytic deposition of
45
46 nickel provides a self-repaired surface with similar properties to the original.
47
48
49
50
51
52
53

54 **Acknowledgements**

55
56
57 The authors acknowledge Mrs Kirstin Andrews for her assistance in fluorescence microscope
58
59 analysis.
60
61
62
63
64
65

The work was financed by the Research Funding from the Edinburgh Napier University.

References

- [1] A.P. Esser-Kahn, S. a. Odom, N.R. Sottos, S.R. White, J.S. Moore, Triggered Release from Polymer Capsules, *Macromolecules*. 44 (2011) 5539–5553. doi:10.1021/ma201014n.
- [2] S.H. Cho, S.R. White, P. V. Braun, Self-Healing Polymer Coatings, *Adv. Mater.* 21 (2009) 645–649. doi:10.1002/adma.200802008.
- [3] S.J. García, H.R. Fischer, P.. White, J. Mardel, Y. González-García, J.M.C. Mol, A.E. Hughes, Self-healing anticorrosive organic coating based on an encapsulated water reactive silyl ester: Synthesis and proof of concept, *Prog. Org. Coatings*. 70 (2011) 142–149. doi:10.1016/j.porgcoat.2010.11.021.
- [4] D.G. Shchukin, H. Möhwald, Smart nanocontainers as depot media for feedback active coatings., *Chem. Commun. (Camb)*. 47 (2011) 8730–8739. doi:10.1039/c1cc13142g.
- [5] D. Fix, D. V. Andreeva, Y.M. Lvov, D.G. Shchukin, H. Möhwald, Application of Inhibitor-Loaded Halloysite Nanotubes in Active Anti-Corrosive Coatings, *Adv. Funct. Mater.* 19 (2009) 1720–1727. doi:10.1002/adfm.200800946.
- [6] M.F. Montemor, Functional and smart coatings for corrosion protection: A review of recent advances, *Surf. Coatings Technol.* 258 (2014) 17–37. doi:10.1016/j.surfcoat.2014.06.031.
- [7] A. Vimalanandan, L.P. Lv, T.H. Tran, K. Landfester, D. Crespy, M. Rohwerder, Redox-responsive self-healing for corrosion protection, *Adv. Mater.* 25 (2013) 6980–6984. doi:10.1002/adma.201302989.
- [8] V. Karpakam, K. Kamaraj, S. Sathiyarayanan, G. Venkatachari, S. Ramu, Electrosynthesis of polyaniline–molybdate coating on steel and its corrosion protection performance, *Electrochim. Acta*. 56 (2011) 2165–2173. doi:10.1016/j.electacta.2010.11.099.

- [9] R. Arefinia, A. Shojaei, H. Shariatpanahi, J. Neshati, Anticorrosion properties of smart coating based on polyaniline nanoparticles/epoxy-ester system, *Prog. Org. Coatings*. 75 (2012) 502–508. doi:10.1016/j.porgcoat.2012.06.003.
- [10] A. Latnikova, D. Grigoriev, M. Schenderlein, H. Möhwald, D. Shchukin, A new approach towards “active” self-healing coatings: exploitation of microgels, *Soft Matter*. 8 (2012) 10837. doi:10.1039/c2sm26100f.
- [11] A. Yabuki, K. Okumura, Self-healing coatings using superabsorbent polymers for corrosion inhibition in carbon steel, *Corros. Sci.* 59 (2012) 258–262. doi:10.1016/j.corosci.2012.03.007.
- [12] T. Nesterova, K. Dam-Johansen, L.T. Pedersen, S. Kiil, Microcapsule-based self-healing anticorrosive coatings: Capsule size, coating formulation, and exposure testing, *Prog. Org. Coatings*. 75 (2012) 309–318. doi:10.1016/j.porgcoat.2012.08.002.
- [13] E.M. Moustafa, A. Dietz, T. Hochsattel, Manufacturing of nickel/nanocontainer composite coatings, *Surf. Coatings Technol.* 216 (2013) 93–99. doi:10.1016/j.surfcoat.2012.11.030.
- [14] D. A. Koleva, N. Boshkov, V. Bachvarov, H. Zhan, J.H.W. de Wit, K. van Breugel, Application of PEO113–b-PS218 nano-aggregates for improved protective characteristics of composite zinc coatings in chloride-containing environment, *Surf. Coatings Technol.* 204 (2010) 3760–3772. doi:10.1016/j.surfcoat.2010.04.043.
- [15] A. Stankiewicz, Z. Jagoda, K. Zielińska, I. Szczygieł, Gelatin microgels as a potential corrosion inhibitor carriers for self-healing coatings: Preparation and codeposition, *Mater. Corros.* 66 (2015). doi:10.1002/maco.201508436.
- [16] J.B. Mallory, G. O.; Hajdu, *Electroless Plating: Fundamentals and Applications*, AESF, Orlando, 1990. http://www.tau.ac.il/~chemlaba/Files/Electroless/12777_01.pdf.
- [17] M.C. Biesinger, B.P. Payne, L.W.M. Lau, A. Gerson, R.S.C. Smart, X-ray photoelectron spectroscopic chemical state Quantification of mixed nickel metal, oxide and hydroxide systems, *Surf. Interface Anal.* 41 (2009) 324–332. doi:10.1002/sia.3026.

- 1
2
3
4
5 [18] J.A. Syed, S. Tang, H. Lu, X. Meng, Smart PDDA/PAA multilayer coatings with enhanced
6 stimuli responsive self-healing and anti-corrosion ability, *Colloids Surfaces A Physicochem.*
7 *Eng. Asp.* 476 (2015) 48–56. doi:10.1016/j.colsurfa.2015.03.021.
8
9
10 [19] M. Islam, T. Shehbaz, Effect of synthesis conditions and post-deposition treatments on
11 composition and structural morphology of medium-phosphorus electroless Ni-P films, *Surf.*
12 *Coatings Technol.* 205 (2011) 4397–4400. doi:10.1016/j.surfcoat.2011.03.042.
13
14 [20] G. Klöck, H. Frank, R. Houben, T. Zekorn, A. Horcher, U. Siebers, M. Wöhrle, K. Federlin,
15 U. Zimmermann, Production of purified alginates suitable for use in immunoisolated
16 transplantation, *Appl. Microbiol. Biotechnol.* 40 (1994) 638–643. doi:10.1007/BF00173321.
17
18
19 [21] M. Fertah, A. Belfkira, E. montassir Dahmane, M. Taourirte, F. Brouillette, Extraction and
20 characterization of sodium alginate from Moroccan *Laminaria digitata* brown seaweed, *Arab.*
21 *J. Chem.* 10 (2017) S3707–S3714. doi:10.1016/j.arabjc.2014.05.003.
22
23
24 [22] D. Snihirova, M. Taryba, S. V. Lamakaa, M. Fatima Montemor, Corrosion inhibition
25 synergies on a model Al-Cu-Mg sample studied by localized scanning electrochemical
26 techniques, *Corros. Sci.* 112 (2016) 408–417. <http://dx.doi.org/10.1016/j.corsci.2016.08.008>.
27
28
29 [23] A. C. Bastos, M. C. Quevedo, O. V. Karavai, M. G. S. Ferreira, Review—On the Application
30 of the Scanning Vibrating Electrode Technique (SVET) to Corrosion Research, *J.*
31 *Electrochem. Soc.* 164 (2017) C973-C990. DOI: 10.1149/2.0431714jes.
32
33
34 [24] I.B. Obot, I. B. Onyeachu, A. Madhan Kumara, Sodium alginate: A promising biopolymer for
35 corrosion protection of API X60 high strength carbon steel in saline medium, *Carbohydr.*
36 *Polym.* 178 (2017) 200-208. <https://doi.org/10.1016/j.carbpol.2017.09.049>.
37
38
39 [25] S. M. Tawfik, Alginate surfactant derivatives as an eco-friendly corrosion inhibitor for carbon
40 steel in acidic environments, *RSC Adv.* 5 (2015) 104535-104550. DOI: 10.1039/c5ra20340f.
41
42
43 [26] A.P. Grosvenor, M.C. Biesinger, R.S.C. Smart, N.S. McIntyre, New interpretations of XPS
44 spectra of nickel metal and oxides, *Surf. Sci.* 600 (2006) 1771–1779.
45
46
47
48
49
50
51
52
53
54
55
56
57
58
59
60
61
62
63
64
65

- 1
2
3
4
5
6
7
8 [27] B. Elsener, D. Atzei, A. Krolkowski, A. Rossi, Effect of phosphorus concentration on the
9
10
11
12
13
14
15
16 [28] J. Okado, M. Shima, I.R. McColl, R.B. Waterhouse, T. Hasegawa, M. Kasaya, Ni-P and Mo:
17
18
19
20
21
22
23
24
25
26
27
28
29
30
31
32
33
34
35
36
37
38
39
40
41
42
43
44
45
46
47
48
49
50
51
52
53
54
55
56
57
58
59
60
61
62
63
64
65
- [27] B. Elsener, D. Atzei, A. Krolkowski, A. Rossi, Effect of phosphorus concentration on the electronic structure of nanocrystalline electrodeposited Ni-P alloys: An XPS and XAES investigation, *Surf. Interface Anal.* 40 (2008) 919–926. doi:10.1002/sia.2802.
- [28] J. Okado, M. Shima, I.R. McColl, R.B. Waterhouse, T. Hasegawa, M. Kasaya, Ni-P and Mo: An excellent fretting wear resistant combination, *Wear.* 225–229 (1999) 749–757. doi:10.1016/S0043-1648(99)00029-0.
- [29] Z. Qi, W. Lee, XPS study of CMP mechanisms of NiP coating for hard disk drive substrates, *Tribol. Int.* 43 (2010) 810–814. doi:10.1016/j.triboint.2009.11.007.
- [30] M.-P.H. Ping-Ho Lo, Wen-Ta Tsai, Ju-Tung Lee, The Electrochemical Behavior of Electroless Plated Ni-P Alloys in Concentrated NaOH Solution Title, *J. Electrochem. Soc.* 142 (1995) 91–96.
- [31] J. Kang, Y. Yang, H. Shao, Comparing the anodic reactions of Ni and Ni-P amorphous alloy in alkaline solution, *Corros. Sci.* 51 (2009) 1907–1913. doi:10.1016/j.corosci.2009.04.032.
- [32] A. Królikowski, P. Butkiewicz, Anodic behavior of NiP alloys studied by impedance spectroscopy, *Electrochim. Acta.* 38 (1993) 1979–1983. doi:10.1016/0013-4686(93)80327-V.

Figure captions

Fig. 1 Steel samples covered with electroplated nickel coating after 24 hours of immersion in 3.5 wt.% NaCl without alginate microgels (bottom sample) and with alginate microgels (top sample).

Fig. 2 Chronoamperometry of the steel samples immersed in the 3.5 wt.% NaCl solution without and with the alginate microgels at an applied potential of + 10 mV vs open circuit potential.

Fig. 3 SEM microphotographs of a) Ni-P coating and b) Ni-P/alginate microgels coating.

Fig. 4 Fluorescence microscope microphotograph of the surface of the Ni-P\ alginate microgels coating.

Fig. 5 Current density changes above a) Ni-P coating surface and b) Ni-P\alginate microgels coating surface after 0, 5, 12, 18 and 20 h immersion in 50mM NaCl detected by SVET.

Fig. 6 Ni $2p_{3/2}$ spectrum for Ni-P coating at as-deposited state. Due to multiplet splitting effects, several peaks are present for each chemical species (NiP (red lines), oxide (blue lines) and hydroxide (green lines) [17]). The fitting envelope is shown with a black line.

Fig. 7 Comparison of the spectra for Ni-P and Ni-P\alginate microgels coatings at their as-deposited state.

Fig. 8 P $2p$ spectra for Ni-P coating at as-deposited state. Two chemical species are identified, phosphide (green lines) and phosphate (purple lines), where the amount of oxidised phosphorus is calculated to be 20%. The fitting envelope is shown with a black line.

Fig. 9 Comparison between the Ni $2p_{3/2}$ spectrum for Ni-P and Ni-P\alginate microgels coatings after 6 h of immersion in 3.5 wt.% NaCl solution. Due to multiplet splitting effects, several peaks are present for each chemical species (NiP (red lines), oxide (blue lines) and hydroxide (green lines) [17]). The fitting envelope is shown with a black line.

Figure 1
[Click here to download high resolution image](#)



Figure 2
[Click here to download high resolution image](#)

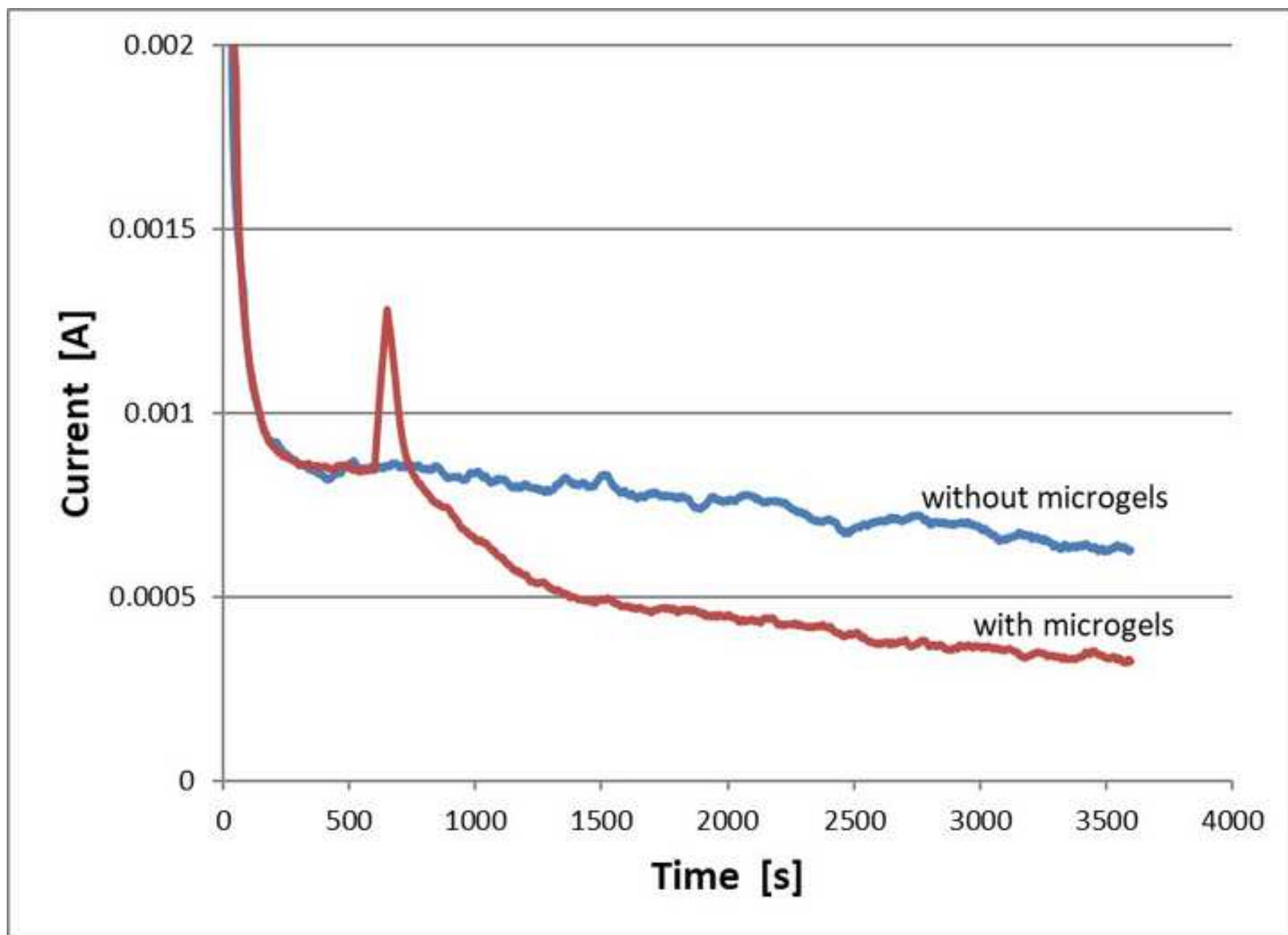
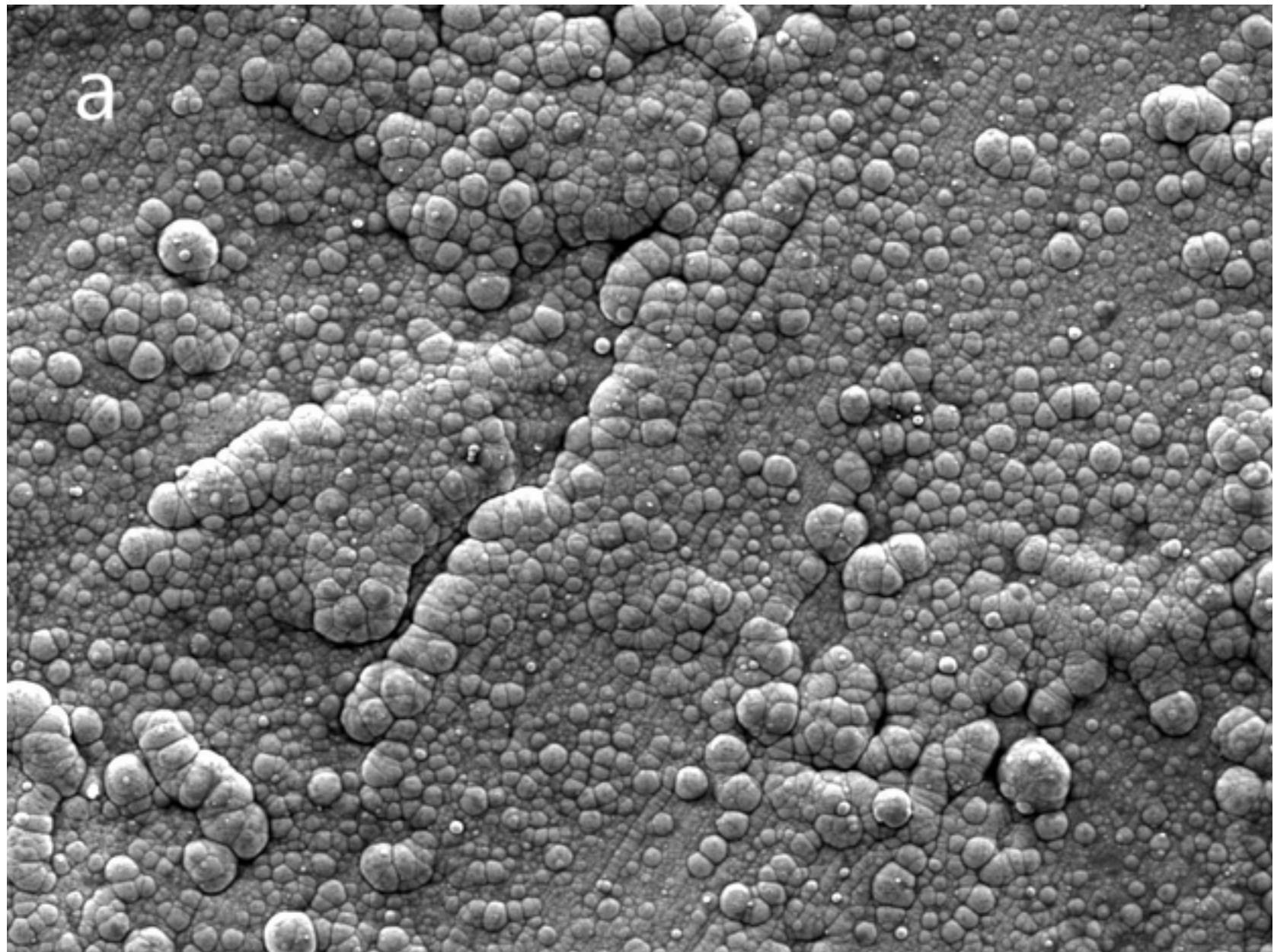


Figure 3a

[Click here to download high resolution image](#)



SEM HV: 15.0 kV

WD: 14.96 mm

VEGA3 TESCAN

SEM MAG: 1.00 kx

View field: 277 μ m

50 μ m

Det: SE

Date(m/d/y): 08/14/17

Edinburgh Napier University

Figure 3b
[Click here to download high resolution image](#)

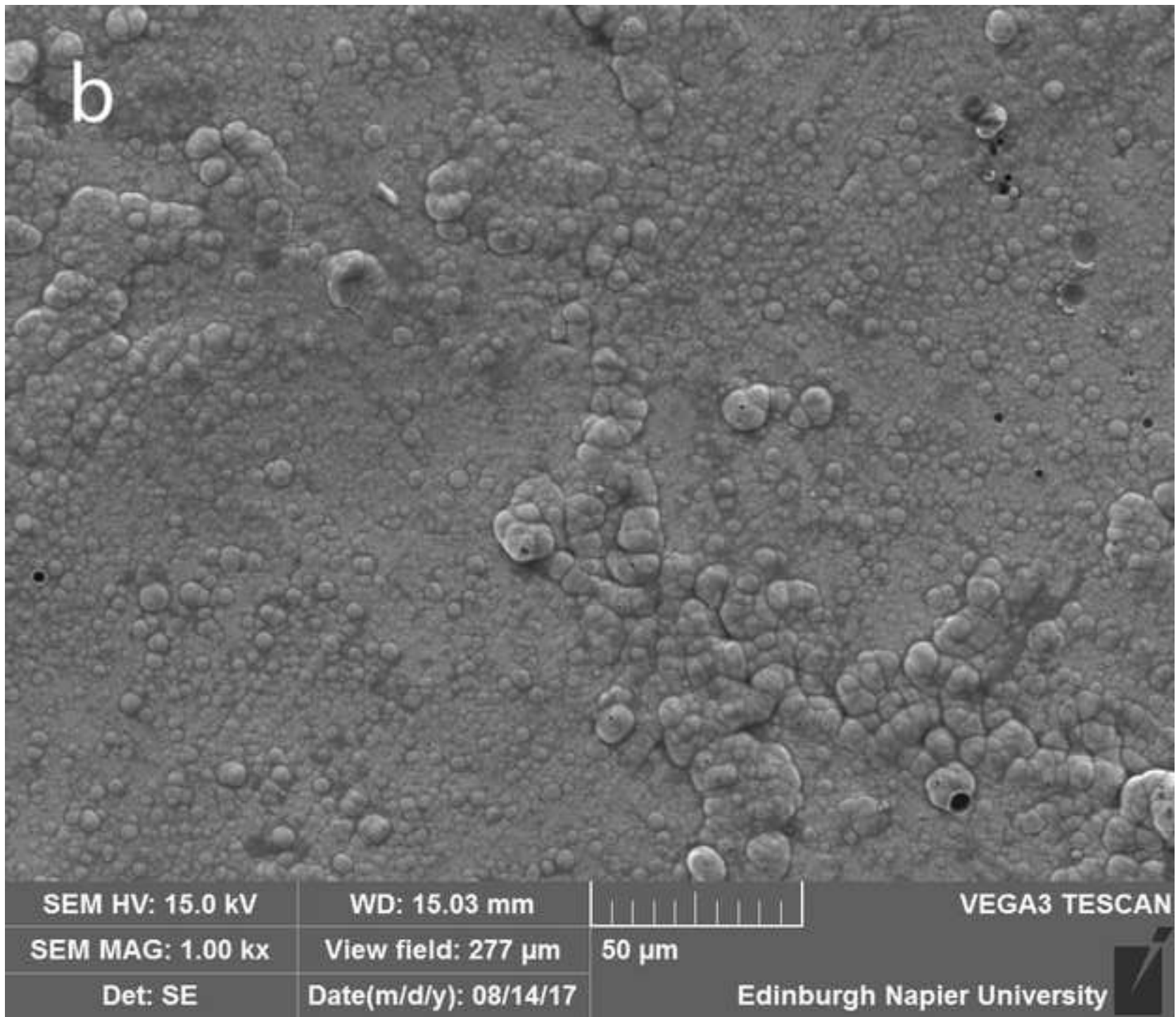


Figure 4
[Click here to download high resolution image](#)

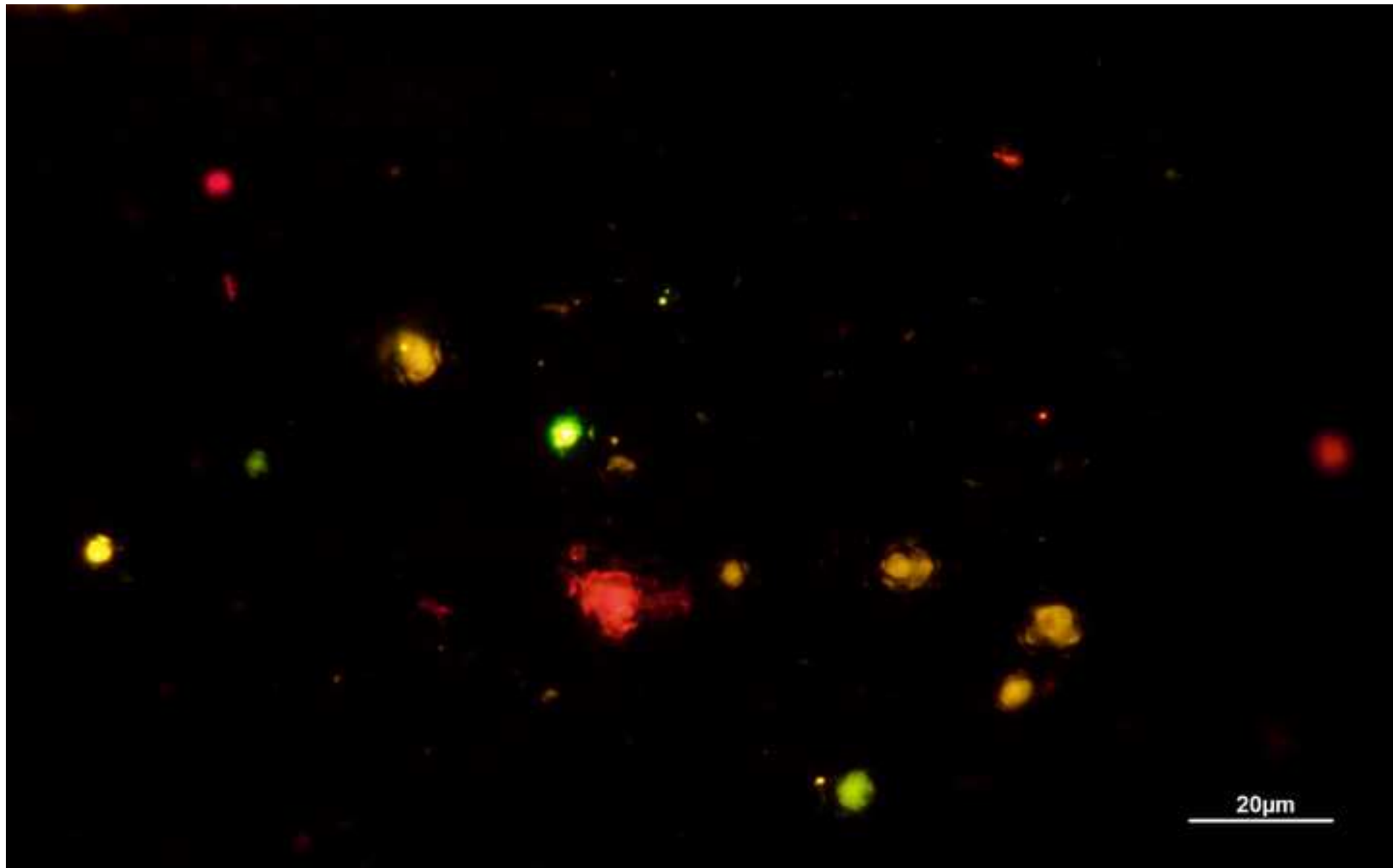


Figure 5a
[Click here to download high resolution image](#)

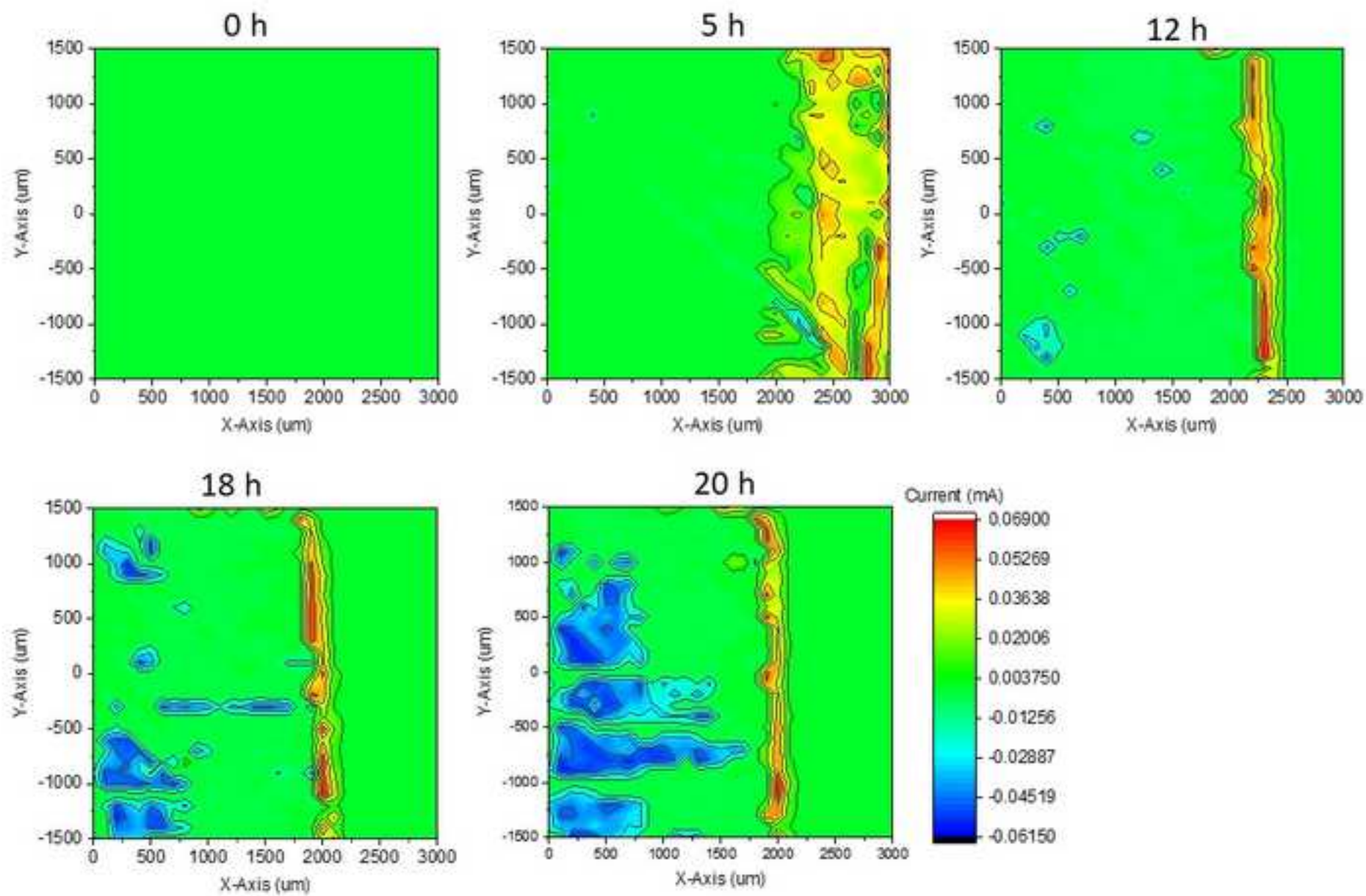


Figure 5b
[Click here to download high resolution image](#)

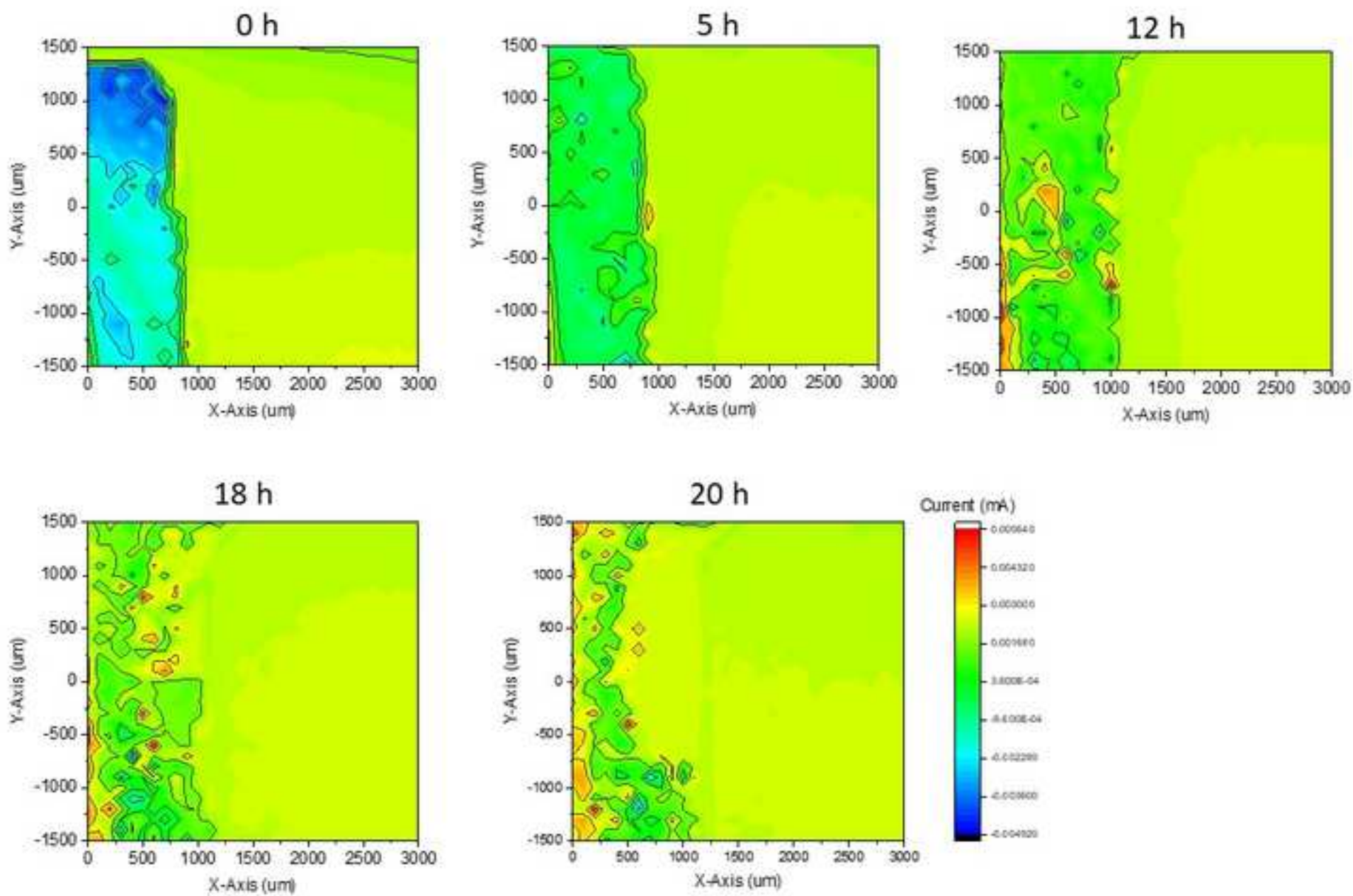


Figure 6
[Click here to download high resolution image](#)

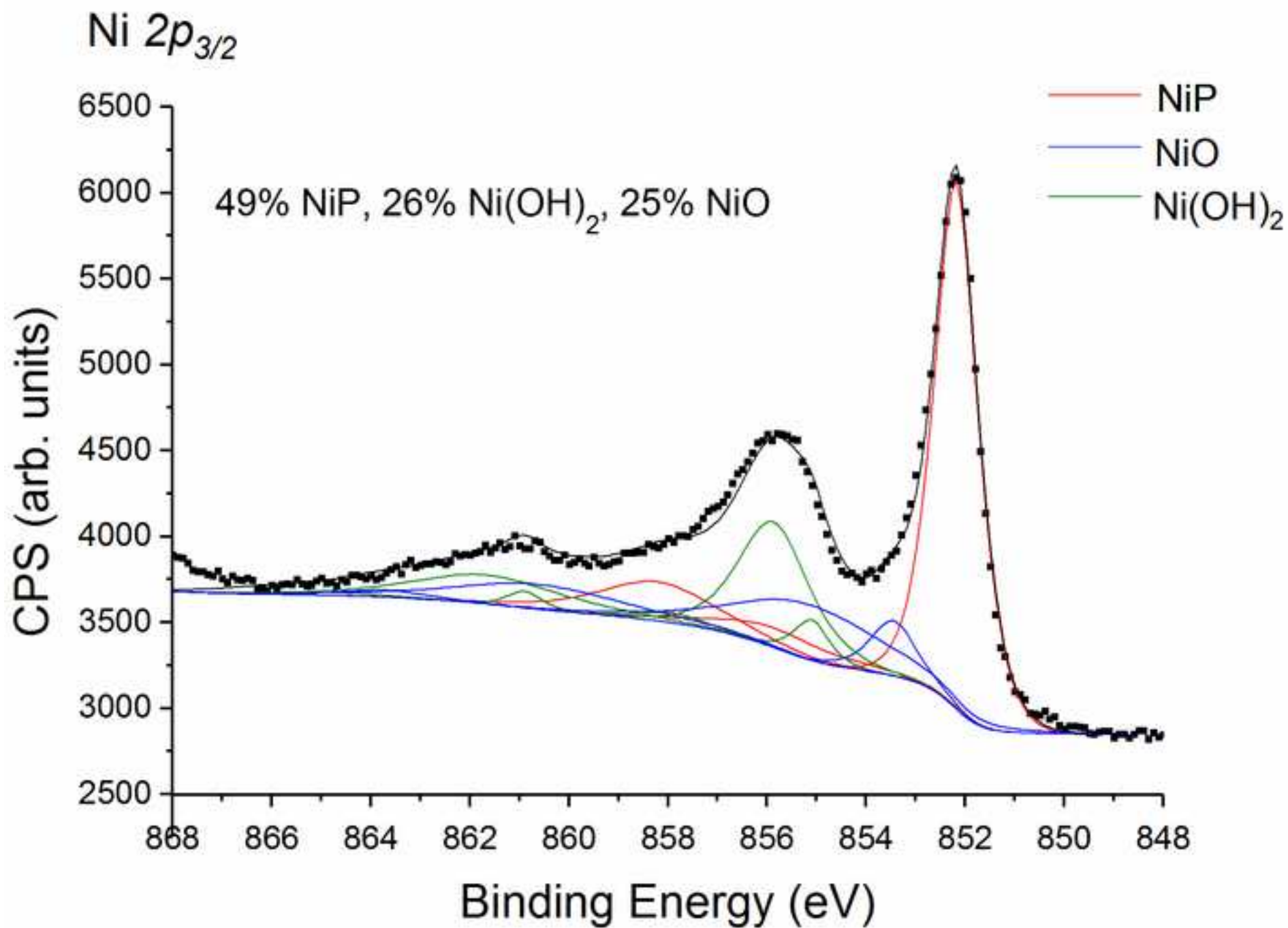


Figure 7
[Click here to download high resolution image](#)

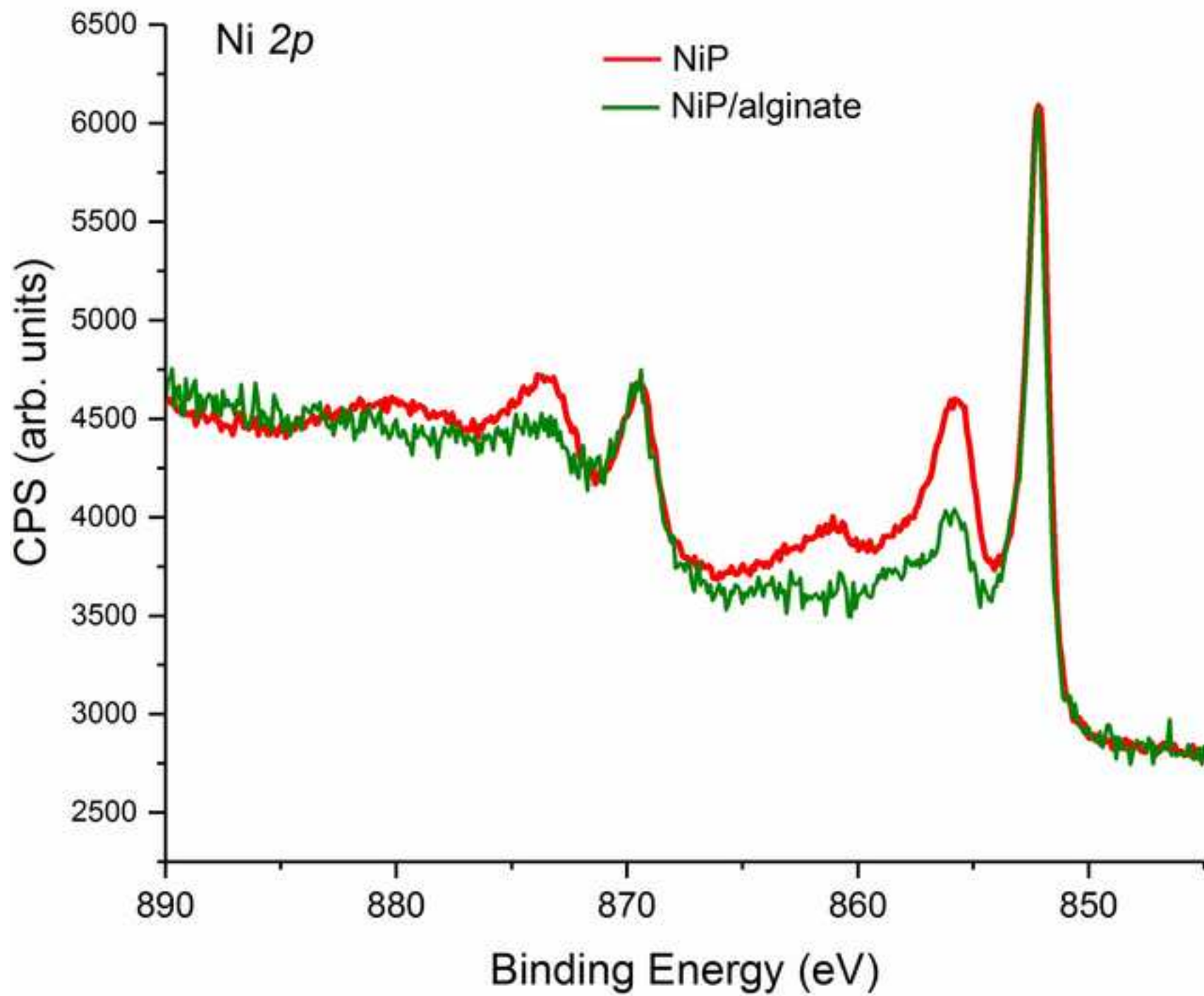


Figure 8
[Click here to download high resolution image](#)

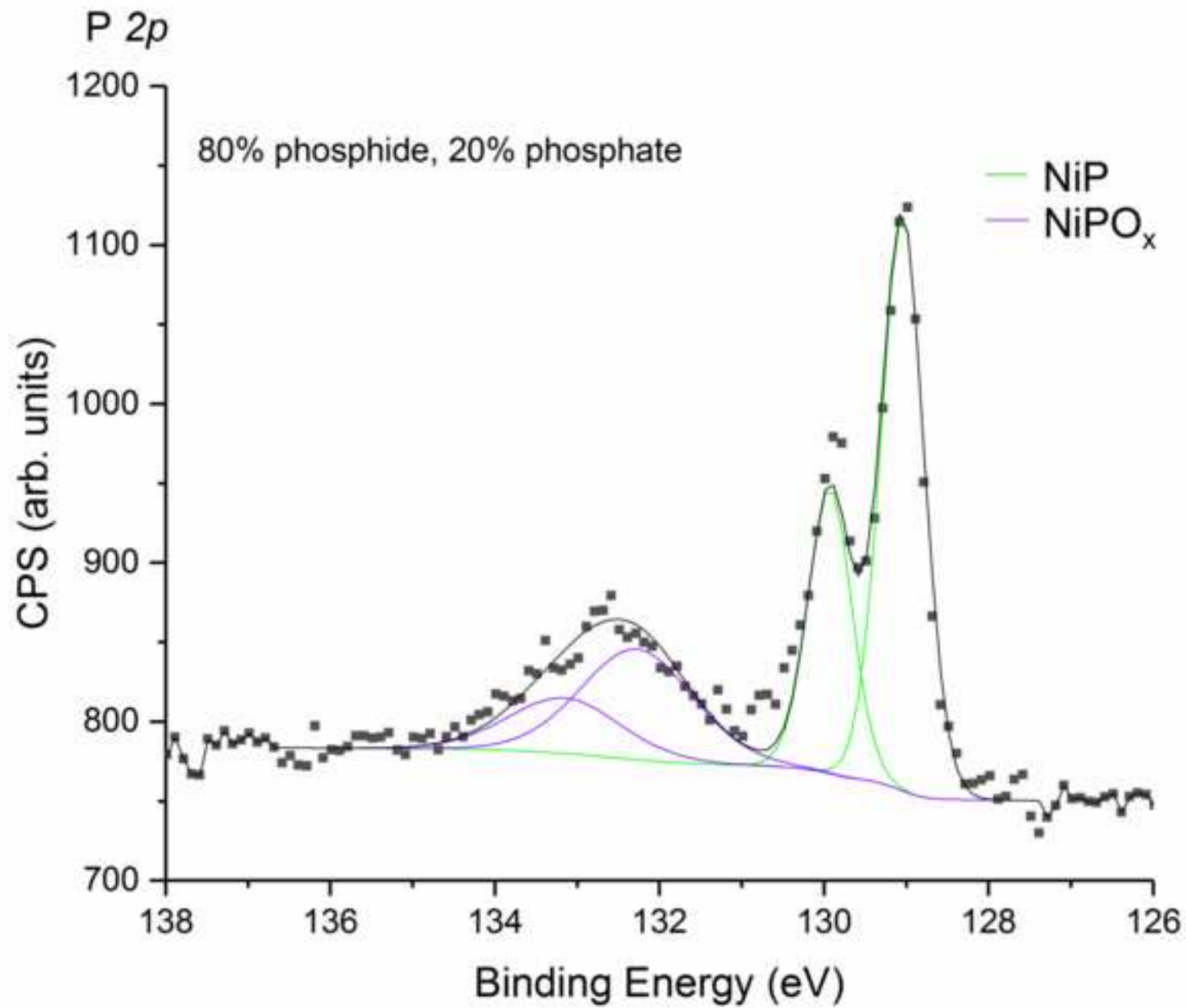
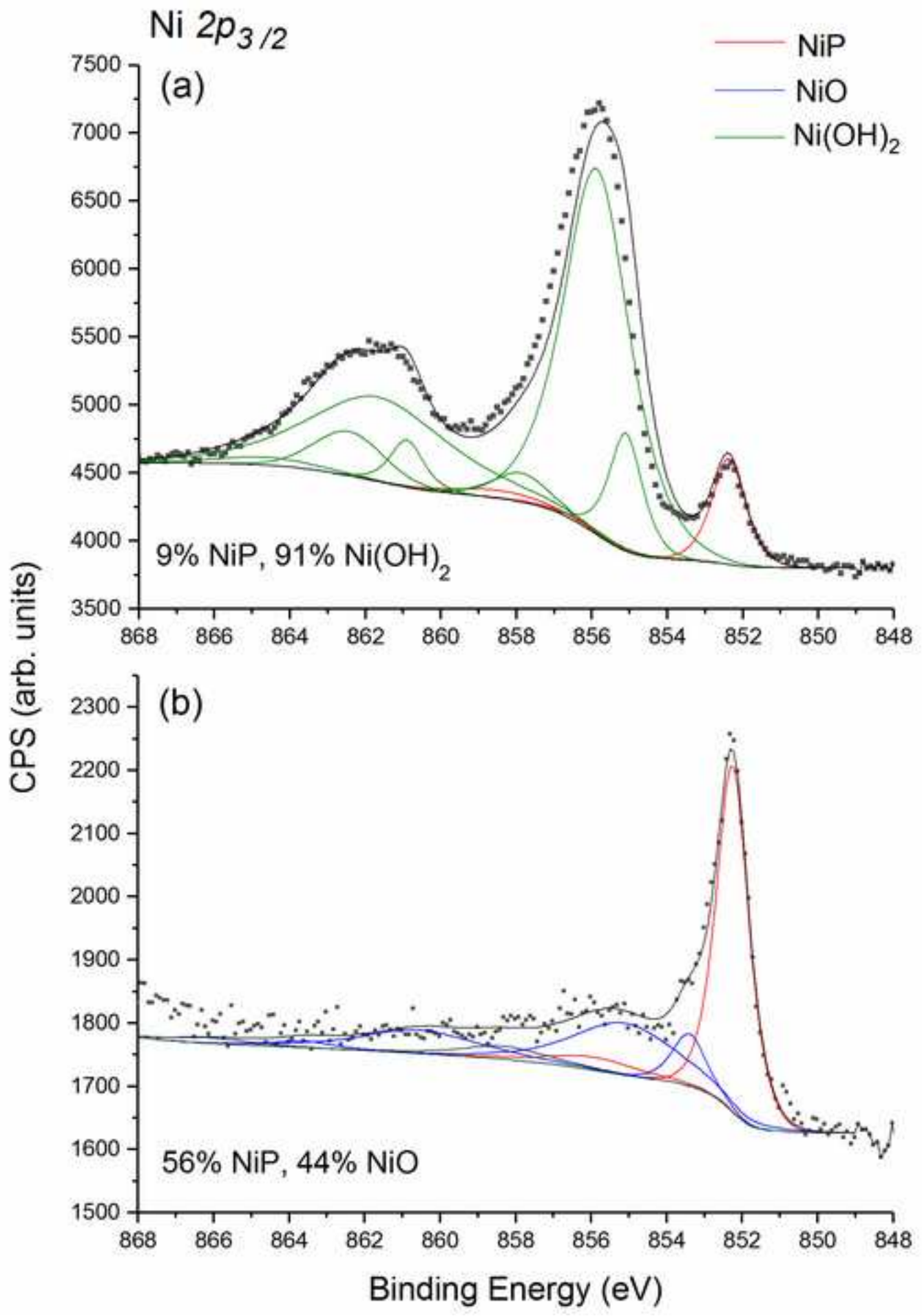


Figure 9

[Click here to download high resolution image](#)



Tables

Table 1. X-ray fluorescence analysis of the steel sample immersed in 3.5 wt.% NaCl solution containing alginate microgels.

time of immersion, h	Fe	Mn	Co	Ni	Cu	Zn	Cr
0	99.5954	0.1543	0.0241	0	0.1718	0.0444	0
1	97.5356	0.2818	0.4194	1.6996	0.0221	0.0307	0
3	97.3933	0.3072	0.4119	1.8578	0.0165	0	0.0033
24	96.8923	0.2954	0.4068	2.3307	0.0307	0.028	0.0062

Table 2. Elemental and chemical analysis of coatings immersed in 3.5 wt.% NaCl solution by XPS (Ni $2p_{3/2}$ and P $2p$).

coating	time,h	chemical analysis, %					elemental analysis, %				Ni:C	Ni:P
		Ni(OH) ₂	NiO	NiP	PO _x	P	C	O	Ni	P		
Ni-P	0	25.95	25.43	48.62	20.38	79.62	74.44	18.12	3.11	4.34	0.042	0.72
	1	44.84	33.32	21.84	20.62	79.38	72.84	23.57	2.10	1.48	0.029	1.42
	6	90.96	0.00	9.04	30.22	69.78	65.56	30.37	2.70	1.36	0.041	1.98
Ni-P\alginate microgels	0	4.70	36.57	58.73	39.34	60.66	92.78	5.23	0.79	1.20	0.008	0.66
	1	0.00	45.02	54.98	29.67	70.33	95.44	2.69	0.53	1.31	0.005	0.40
	6	0.00	44.38	55.62	20.78	79.22	95.25	3.07	0.57	1.11	0.006	0.51